ISSN 2616-5767 Vol.8, Issue 4: 94-101, DOI: 10.25236/AJETS.2025.080413

Innovative Design and High Mobility of Intelligent Security Robot Chassis Based on Independent Drive of Servo Motor Wheel Set

Yan Li[#,a,*], Xianyu Xin[#]

School of Mechanical and Electrical Engineering, Shandong Jianzhu University, Jinan, China, 250101
[a]liyan20030904@163.com
[#]These Authors Contributed Equally

Abstract: *This study focuses on the innovative design and high mobility of intelligent security robot chassis, proposing a design scheme based on independent drive of servo wheel sets. The McNaught wheel omnidirectional motion system is adopted, enabling independent drive of steering wheels and drive wheels to achieve high-speed movement and agile turning in complex environments. The STM32F4 chip is used as the controller, integrating CAN bus communication and power, drive, and sensor modules. Structurally, the wheel system is optimized with expansion sleeves to enhance concentricity, and carbon fiber plates are used for lightweight design to improve stability. The gimbal mounting bracket undergoes finite element analysis to ensure structural integrity under extreme conditions. Functionally, the system integrates multiple sensors and camera devices, utilizing SLAM technology to achieve panoramic perception, autonomous obstacle avoidance, and mapping. Experiments show that the chassis has a minimum safety factor of 15 and a maximum displacement of 0.001932 mm, meeting application requirements. It provides technical support for security patrols in complex environments such as commercial plazas, demonstrating high application and promotional value. Intelligent security robots are equipped with functions such as high-speed movement, agile direction change, flexible turning and in-place rotation, which can meet the needs of various complex working environments.*

Keywords: *Intelligent Security Robot; Chassis Design; Mecanum Wheels; High Mobility*

1. Introduction

In recent years, the integration and innovation of new-generation information technologies such as artificial intelligence, the Internet of Things, cloud computing, and big data have injected strong momentum into the development of robotics technology. As an important application branch, intelligent security robots leverage deep learning algorithms for precise target recognition and behavior analysis, utilize the IoT for real-time interaction of multi-source data, and employ cloud computing and big data for efficient data processing and intelligent decision-making. Currently, they are widely applied in scenarios such as transportation hubs, industrial parks, and emergency rescue [1], serving as a key driving force for the intelligent upgrading of modern security systems.

Zhang et al. [2] proposed a threshold-free alarm algorithm based on energy feature transformation. By extracting the energy, fluctuation, and time features of monitored data and integrating a random forest algorithm to construct a model, the algorithm achieves automated alarms for inspection software. This method combines high accuracy with efficiency, significantly reducing IDC maintenance costs ; Xu et al. [3] designed a factory security patrol robot based on the STM32F407ZGT6 microcontroller and Raspberry Pi 4 Model B image processing unit, integrating cameras, RFID sensors, and other devices. She developed visual perception and positioning detection modules to enable the robot's autonomous navigation and recognition/detection capabilities ; Liu et al. [4] employed Simultaneous Localization and Mapping (SLAM) technology, combined with lidar and odometry, to achieve localization, mapping, and navigation functions; Li et al. [5] used a lightweight version of the YOLOv8n algorithm, employing GhostNet for lightweight improvements to YOLOv8n, aiming to reduce computational load and memory consumption while enhancing target detection speed . However, while security robots have numerous advantages, they also have certain limitations. Currently, most security robots are large and bulky, constrained by mechanical structure, power systems, and load weight, resulting in relatively slow movement speed, turning speed, and maneuverability. This limitation makes it difficult for them to quickly reach designated locations or adjust their direction of travel in response to sudden situations or scenarios requiring rapid response, thereby affecting response efficiency and limiting their application in scenarios with high mobility requirements.

To address this issue, this intelligent security robot features an innovative chassis design with servo wheel assemblies, where the steering wheels and drive wheels are driven by independent motors, enabling high mobility. The drive wheels are equipped with M3508 brushless DC motors, using D-shaped shaft clamping transmission to ensure rapid movement; the steering wheels are fitted with M6020 motors, achieving agile steering through mosquito coil plate transmission. The dual-motor independent drive mode grants the robot multi-degree-of-freedom movement capabilities, supporting on-the-spot rotation and intelligent obstacle avoidance, ensuring flexible control in complex scenarios. Additionally, the unique wheel self-locking [6] technology enhances traction, while the gas spring preload design improves chassis stability, balancing load-bearing performance and movement safety, effectively addressing the issue of slow movement in traditional security robots.

2. Research Content

The research focus of this paper revolves around the following points: Among them, the product described in this paper has diverse application scenarios and holds significant practical value in security patrol operations within complex environments such as commercial plazas, train stations, bus stations, airports, and schools.

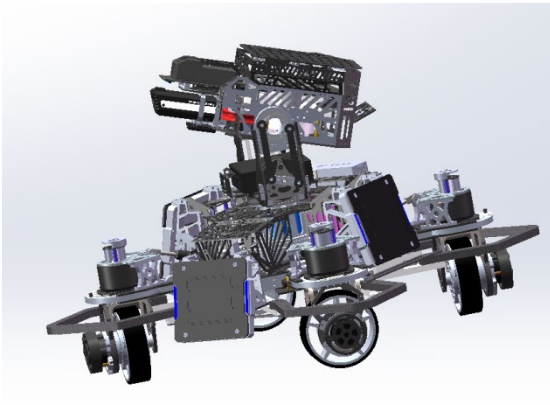

Figure 1 Schematic diagram of the motion chassis system and gimbal system

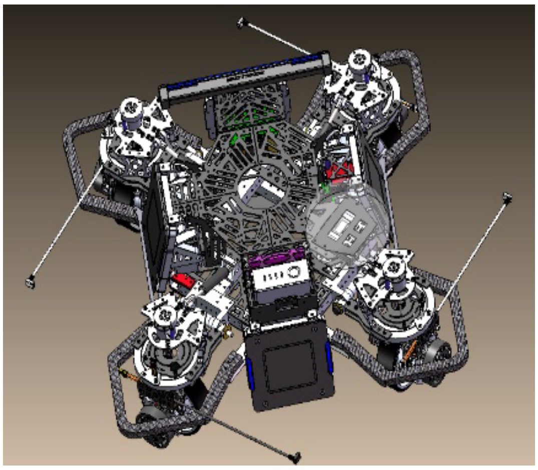

Figure 2 Sports chassis system

Component Selection: The security robot described in this paper consists of a mobile chassis system and a pan-tilt system, with the overall design shown in Figure 1. The structural diagram of the mobile chassis system is shown in Figure 2. The mobile chassis is used to carry the pan-tilt system and move it according to received command signals, transporting the pan-tilt system to the designated scene. The mobile chassis system includes: a control system using an STM32F4 chip as the controller; communication between the main control board housing the chip and various drive components employs a CAN bus, connected to power modules, DC motor drive modules, real-time video capture modules,

ISSN 2616-5767 Vol.8, Issue 4: 94-101, DOI: 10.25236/AJETS.2025.080413

GPS positioning modules, infrared sensors, ultrasonic sensors, explosion-proof impact components, etc. The hardware framework of the intelligent security robot provided in this paper is shown in Figure 3; It also includes: a wheel system composed of steering wheels and drive wheels. The steering wheels are driven by L289N DC motor drive boards to power DC brushless reduction motors, while the drive wheels use M3508 DC brushless motors, driven via D-shaped shaft clamping transmission. These motors have a continuous power of 150W and a continuous torque of 2.8N•m, enabling rapid movement to drive the four independently moving Mecanum wheels [7]. The wheel arrangement configurations of the McNaughton wheel omnidirectional motion system are diverse, enabling forward movement, lateral movement, diagonal movement, rotation, and combinations thereof.

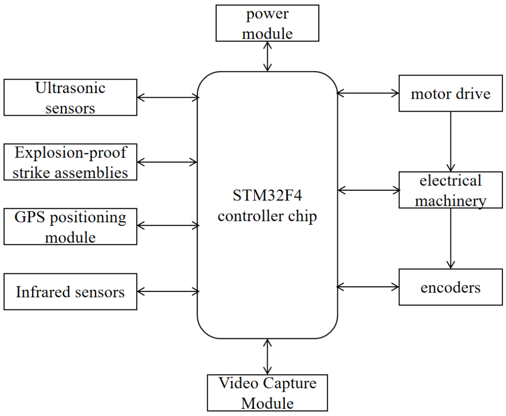

Figure 3 Security robot hardware framework

The gimbal system includes: a camera mechanism and an ammunition launch mechanism. The camera mechanism is mounted on the neck of the gimbal, as shown in Figure 4. It includes a primary camera and a secondary camera. The primary camera automatically searches for and identifies targets, producing 60 frames per second of real-time video that is transmitted to the backend. The transmission process connects to the STM32 chip via a serial port communication over a wireless network, enabling remote viewing of video information and timely transmission of commands to smart devices such as PCs. The ammunition launch mechanism is shown in Figure 5.

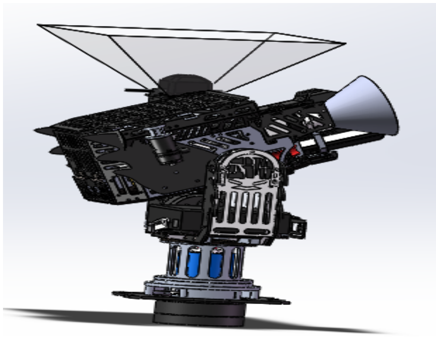

Figure 4 camera system

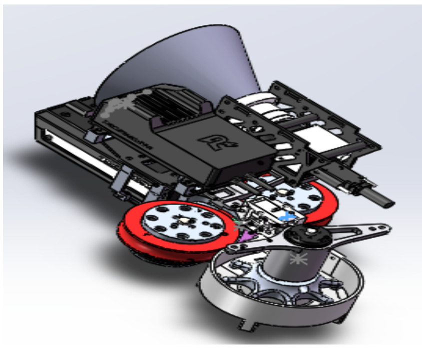

Figure 5 Ammunition firing mechanism

In the technical design phase of the product described in this paper, the algorithm for visual data collection by the main camera was optimized to ensure functional reliability and practicality. The main camera is primarily used to identify and detect certain exposed hazardous items, which serve as features for determining security targets. The hazardous item selected in this paper is a dagger. First, a knife image database was created and trained using the VOC2007 dataset format. The created dataset was iteratively trained 20,000 times on a GTX1050 environment to identify target features, followed by detection and target selection. This enabled the security robot in this paper to achieve knife recognition functionality in its visual module. This method falls under supervised learning-based recognition techniques.

3. Technical Content

The functional implementation principle of the intelligent security robot described in this article is as follows: video images are dynamically captured through an industrial USB camera, and various sensors extract information about the surrounding environment. This information is then transmitted to a mobile client via Internet network WiFi technology. The client can control the robot's behavior based on the video and data fed back by the robot, focusing on observing and tracking “warning” targets, and using “bombing” or electric shock attacks against targets that have already exhibited dangerous behavior. The information transmission process during implementation is shown in Figure 6.

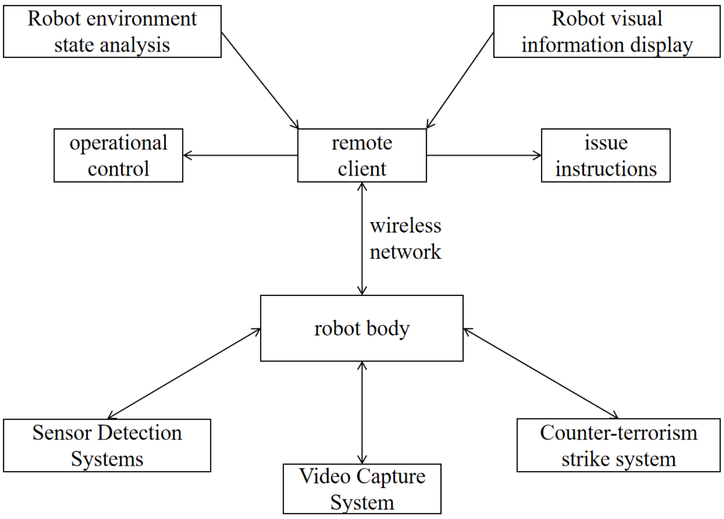

Figure 6 Functional implementation schematic diagram

3.1 Circuit Technology Approach

The vehicle is equipped with two capacitor groups: a supercapacitor group and a surge absorption capacitor group. The supercapacitor array, with its protective circuitry, has parameters of 15.9V/15F, a rated capacity of 1896.075J, and an operating voltage range of 7V to 15.5V; the surge absorption capacitor array has parameters of 50V/20mF, a rated capacity of 25J, and an operating voltage range of 24V to 50V. Regarding the onboard modules, the supercapacitor charging module is used to charge the supercapacitor [8], with a maximum designed power of 120W; the supercapacitor boost module can boost the supercapacitor to an output of 26V, with a maximum designed power of 480W; the NUC power supply module provides power to the NUC, with a maximum designed power of 200W; and the IMU module is used to precisely obtain the robot's posture to enhance movement accuracy.

3.2 Hardware Design

3.2.1 Supercapacitor

To achieve ultra-power mode, this system adopts a general topology structure (as shown in Figure 7), which offers advantages such as convenient power synthesis between the capacitor and the control system, and good fault tolerance during topology switching. The main power paths include two: first, the current passes through the current detection module, high-side switch, and surge absorption module before directly powering the chassis motor; Second, the current first passes through the current detection module and supercapacitor charging module to charge the supercapacitor module, then the supercapacitor supplies power to the chassis motor via the boost module, high-side switch, and surge absorption module. Installation test data indicates that under the condition of limiting the battery output power to no more

ISSN 2616-5767 Vol.8, Issue 4: 94-101, DOI: 10.25236/AJETS.2025.080413

than 50W, after integrating the supercapacitor management module, the power management test module can maintain the battery's 50W output power while continuously providing 120W of power output for 17 seconds.

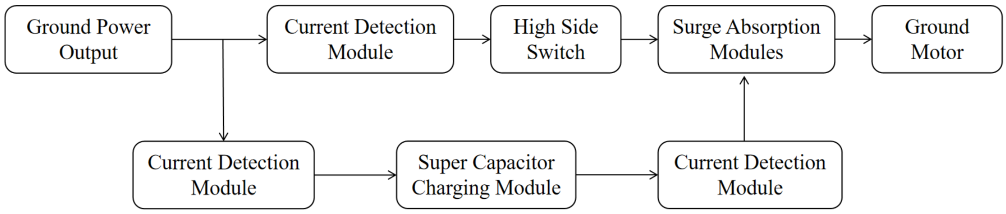

Figure 7 General topology diagram

3.2.2 Controller Module

The controller module serves as the core computational and control unit of the supercapacitor management system, responsible for regulating the operational status of other submodules. The controller employs the STMicroelectronics STM32H750VBT6 chip, which is based on the Cortex-M7 core architecture. It features a six-stage dual-issue superscalar pipeline, a branch predictor, single/double-precision floating-point units, tightly coupled memory (TCM), L1 cache, a digital signal processing (DSP) module, and a memory protection unit (MPU). Operating at a 480MHz clock frequency, the chip achieves approximately 1027 DMIPS of computational performance, providing efficient computational support for the system.

Due to limitations in the number of conductive slip ring lines, independent communication channels cannot be expanded. Therefore, the microcontroller is bridged between the control system and the vehicle controller rmcontrols, using the UART communication protocol to achieve data exchange. The topology architecture after bridging is shown in Figure 8. Communication data packets are appended to the control system data packets for transmission, with the data format strictly adhering to the medium-capacity data transmission protocol standard to ensure the standardization and reliability of data transmission.

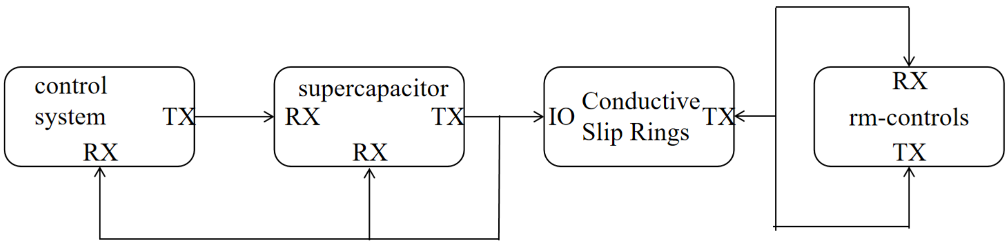

Figure 8 Bridged topology

3.2.3 Supercapacitor Module

The capacitor module uses 2.7V/30F capacitor cells, arranged in a configuration of three parallel and six series modules, with the module's rated parameters being 16.2V/15F. As shown in Figure 9, since the supercapacitor cells use a comparator with a threshold of 2.65V for protection, when an overvoltage occurs in a cell, the comparator outputs a high level to control the N-MOSFET to open. Therefore, the supercapacitor module with cell protection achieves new nominal parameters of 15.9V/15F, with a nominal energy capacity of 1896.075J. The discharge circuit is a series configuration. When a cell triggers discharge, it always discharges to the next cell in the series until the last capacitor in the series discharges to GND. The advantage of this design is that it does not directly waste all the energy during cell charging balancing, thereby improving efficiency. The disadvantage is that the last discharge MOSFET always bears the largest discharge current until all capacitors in the series have equal voltages. During use, this causes heat to concentrate at one end of the module. In such cases, the module should be arranged in a cross pattern during layout to reduce this effect.

The discharge resistors are composed of two 2512-package 4.7Ω resistors stacked together, with each resistor having a power dissipation of 2W. Therefore, due to the influence of the discharge resistors, the total continuous discharge capacity of the module is 53.82W, requiring enhanced heat dissipation to ensure the module's continuous stable operation.

ISSN 2616-5767 Vol.8, Issue 4: 94-101, DOI: 10.25236/AJETS.2025.080413

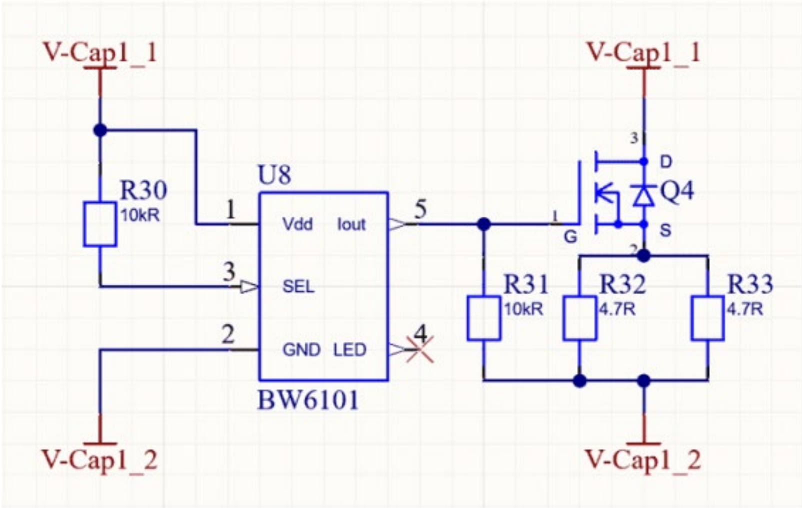

Figure 9 Supercapacitor Cell Protection Circuit Schematic Diagram

4. Finite Element Analysis of Core Components and Gear System Structure

A mechanical performance analysis was conducted on the integrated gimbal mounting bracket, with boundary conditions set as four bolts fixed to a cylindrical surface. Under the vehicle body's horizontal motion conditions, the applied load conditions include: a 200N vertical downward unidirectional force, a 1300N vertical upward unidirectional force, and a 200N·m torque equivalent to that generated by a 2kg mass under a 10m/s² acceleration condition. This load combination is used to simulate the vertical component forces and moments acting under impact conditions such as vehicle ramping.

Based on the simulation results shown in Figure 10(a), the minimum safety factor of the mounting bracket reaches 15. Given that the load amplitude under actual operating conditions is significantly lower than the simulation set value, and the current safety factor indicates that it has the capacity to withstand 15 times the current load, it is determined that the structural strength of this part meets the requirements of actual application. Under extreme conditions such as flying over a slope, the risk of fracture failure at the connection between the gimbal yaw axis and the chassis is low.

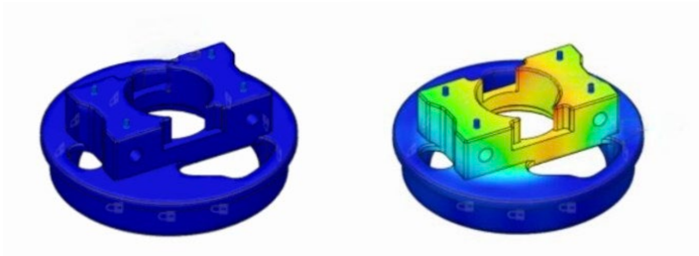

(a) Safety factor chart *(b) Displacement diagram*

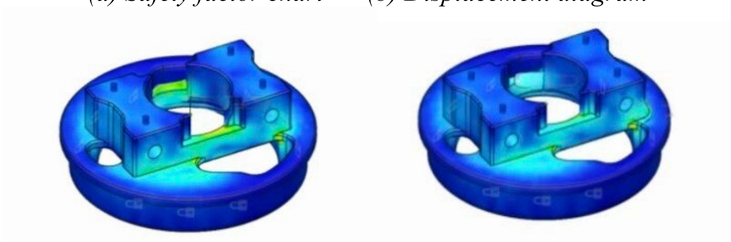

(c) Stress diagram *(d) Strain diagram*

Figure 10 Mechanical properties analysis chart

Referring to the analysis results shown in Figure 10(b), under the same load conditions and boundary conditions, when the vehicle body is in a horizontal motion state, the finite element simulation shows that the maximum displacement of the mounting bracket is 0.001932 mm, indicating that its structural stiffness effectively meets the actual operational requirements and ensures that no vibration of the gimbal will occur due to insufficient stiffness under conventional horizontal motion conditions.

In the conditions shown in Figures 10(c) and 10(d), with the threaded holes on the bottom surface of the mounting bracket serving as fixed constraint boundaries, a vertical downward unidirectional force of 20 N is applied to the lower surfaces of the four bolt holes on both sides while the vehicle body is in a horizontal stationary state. Simulation results show that the maximum stress value of the mounting bracket is 8.277 MPa, with the maximum strain approaching zero. All mechanical performance indicators comply with design specifications.

In the optimization of mechanical transmission structures, the snap ring and washer at the motor output shaft are removed so that the thrust bearing acts directly on the outer ring of the bearing. The original inner-side bearing, model 10-22-6, is replaced with an angular contact bearing of the same specifications. Additionally, thrust ball bearings with dust covers are selected. This structural design effectively reduces the complexity of gear system maintenance, as the dust cover integrates the three-piece thrust ball bearing into a single unit, significantly enhancing the convenience of gear system installation.

The omnidirectional wheel drive system uses an expansion sleeve connection method to secure the omnidirectional wheel flange to the motor output shaft. The omnidirectional wheel flange has six M4 threaded holes, and six M4 screws are sequentially passed through two layers of omnidirectional wheel mounting plates and spacer blocks to achieve a secure connection with the omnidirectional wheel flange. This design significantly simplifies the disassembly and assembly process of the omnidirectional wheel. Additionally, the inner contour of the omnidirectional wheel and the outer contour of the flange's cylindrical section are designed with an interference fit, ensuring high-precision concentricity between the omnidirectional wheel and the motor output shaft.

In terms of omnidirectional wheel component selection, the 6-inch low-hardness omnidirectional wheel rollers from Hangfa are chosen, which form a high-friction coefficient contact with the floor mat surface, effectively enhancing movement stability. The hub structure uses three layers of carbon fiber plates to replace the original aluminum alloy material. By clamping the roller shaft, this design not only significantly reduces the risk of hub deformation due to impact during takeoff and landing but also achieves lightweight design objectives, optimizing the overall machine's mass distribution. The wheel system cross-section diagram is shown in Figure 11.

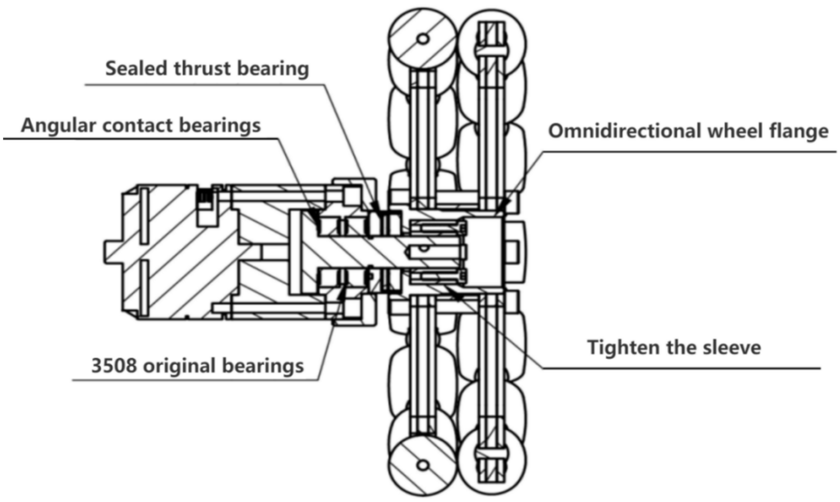

Figure 11 Gear profile diagram

5. Conclusion

The intelligent security robot is equipped with high-speed mobility, agile directional changes, flexible turning, and on-the-spot rotation capabilities. The steering wheels and drive wheels of its chassis servo wheel assembly are each fitted with independent motors.

The drive wheels utilize M3508 brushless DC motors, which employ D-shaped shaft clamping transmission to ensure continuous power for rapid movement; the steering wheels are equipped with M6020 motors, utilizing mosquito coil plate transmission to achieve high rotational efficiency. Since the steering and drive systems of the steering wheel assembly are independent, the robot gains multi-degree-of-freedom movement capabilities, along with obstacle avoidance functionality and the ability to rotate

ISSN 2616-5767 Vol.8, Issue 4: 94-101, DOI: 10.25236/AJETS.2025.080413

in place. This ensures stable and reliable chassis load-bearing performance, effectively avoiding damage to the motors caused by special operating conditions such as steep slopes. Additionally, the unique wheel self-locking structure generates strong traction, while the gas spring preload device further enhances chassis operational stability.

This security robot integrates multiple types of sensors and camera equipment, enabling 360-degree panoramic environmental perception and precise obstacle avoidance. Sensors are distributed at the front, rear, and sides of the robot. The main camera uses a stereo camera, while the auxiliary camera is equipped with a wide-angle camera. A texture projector can be added according to actual application requirements to enhance 3D perception capabilities in low-light environments. Based on sensor data, the robot can use SLAM navigation technology to perform real-time positioning and map construction, enabling autonomous obstacle avoidance.

In terms of mechanical structure design, the robot adopts a quadruped configuration driven by DC motors, with each drive unit equipped with a reducer to output high-torque power. This design enables the robot to perform forward movement, lateral movement, backward movement, and on-the-spot rotation, as well as diverse gaits such as crawling and pacing, demonstrating high mobility flexibility. In terms of environmental adaptability, the product achieves an IP54 waterproof rating and can operate stably within a temperature range of -20°C to 45°C, meeting the demands of various harsh working environments.

Simulation analysis has verified that the minimum safety factor of the robot's critical components reaches 15, meaning it can withstand at least 15 times the current load. This ensures sufficient structural strength in real-world applications, significantly reducing the risk of fracture at the connection point between the gimbal yaw axis and the chassis during slope operations. Finite element simulation results show that the maximum displacement of the component is only 0.001932 mm, indicating excellent rigidity performance, effectively preventing gimbal vibration issues caused by insufficient rigidity during horizontal movement. The intelligent security robot boasts excellent movement performance, perception capability, and structural reliability, enabling it to adapt to complex working environments. In the future, technical upgrades can be made to enhance decision-making accuracy, extend battery life, and expand applications, thereby strengthening its security effectiveness.

References

[1] Song X. Mingming R: Specialized Robots Strengthening Public Safety Defenses [J]. Robot Industry, 2025, (01): 31-35.
[2] Zhang C, Li Zhi F, Tao Y, et al. Design of an IDC Security Patrol Robot Network Monitoring and Alarm System [J]. Mechanical Manufacturing and Automation, 2024, 53(06): 262-267.
[3] Xu H, Xu Y, Sun T, et al. A Discussion on the Design of a Control System for Factory Security Patrol Robots [J]. China Equipment Engineering, 2024, (19): 106-108.
[4] Liu X, Hu B. Design of an Intelligent Patrol Robot System for Indoor Scenarios [J]. Electronic Manufacturing, 2025, 33(10): 43-46.
[5] Li J, Liu B, Zhang Q, et al. Research on Robot Autonomous Patrol Control System Combining Improved YOLOv8n and SLAM [J]. Sensors and MicroSystems, 2024, 43(08): 16-20.
[6] Lin Y. A Adjustable Balance Cart for Slopes [J]. China Science and Technology Information, 2019, (17): 66-67.
[7] Wang X, Zhang L, Wu N, et al. Design and Analysis of Rollers for Vehicle-Mounted McNaughton Wheels [J]. Beijing Automobile, 2025, (02): 16-19+46.
[8] Dong L , Zhang R , Liu X ,et al.High climbing and obstacle-crossing performance intelligent tracked inspection robot for cable trenches[J].Industrial Robot: The International Journal of Industrial and Service Robotics, 2025, 52(1).DOI:10.1108/IR-04-2024-0184.